Supporting Information for "A Cautionary Tale: small earthquakes that might have changed our understanding of Tibetan geodynamics — but were mis-located"

T.J. Craig[1], J.A. Jackson[2], K.F. Priestley[2], G. Ekström[3]

[1]COMET, Institute of Geophysics and Tectonics, School of Earth and Environment, University of Leeds, Leeds, LS2 9JT, UK.

[2]Department of Earth Sciences, University of Cambridge, Cambridge, CB3 0EZ, UK.

[3]Lamont-Doherty Earth Observatory of Columbia University, 61 Route 9W, Palisades, NY 10964, USA

Contents of this file

1. Figures S1 – S11

2. Tables S1 – S2

Introduction

• Figure S1 — Station distribution at regional distances for the 2005/8/20 event.

• Figure S2 — Broadband waveforms and synthetics for the 2005/8/20 event.

• Figure S3 — Station distribution at regional distances for the 2003/2/11 event.

• Figure S4 — Broadband waveforms and synthetics for the 2003/2/11 event.

• Figure S5 — Station distribution at regional distances for the 2005/3/26 event.

• Figure S6 — Teleseismic array analysis for the 2005/3/26 event.

• Figure S7 — Station distribution at regional distances for the 2008/6/19 event.

- Figure S8 — Broadband waveforms and synthetics for the 2008/6/19 event.
- Figure S9 — Surface wave analysis from station IC.WMQ.
- Figure S10 — Surface wave analysis from station IC.QIZ.
- Figure S11 — Surface wave analysis from station IC.XAN.
- Table S1 — Centroid-moment tensor solutions for all four earthquakes reanalysed using the modern gCMT approach.
- Table S2 — Principal axes and best-double couple parameters following reanalysis using the modern gCMT approach.

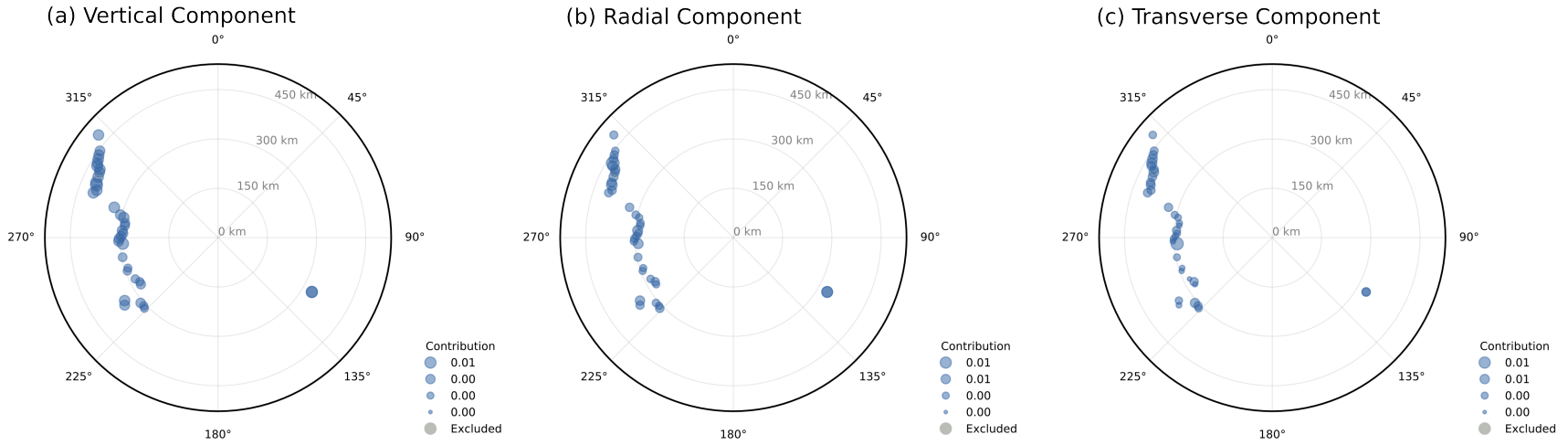

Figure S1. Distribution of stations used in regional waveform inversion for the earthquake on 2005/8/20. (a) Stations contributing vertical component waveforms. (b) Stations contributing radial component waveforms. (c) Stations contributing transverse component waveforms.

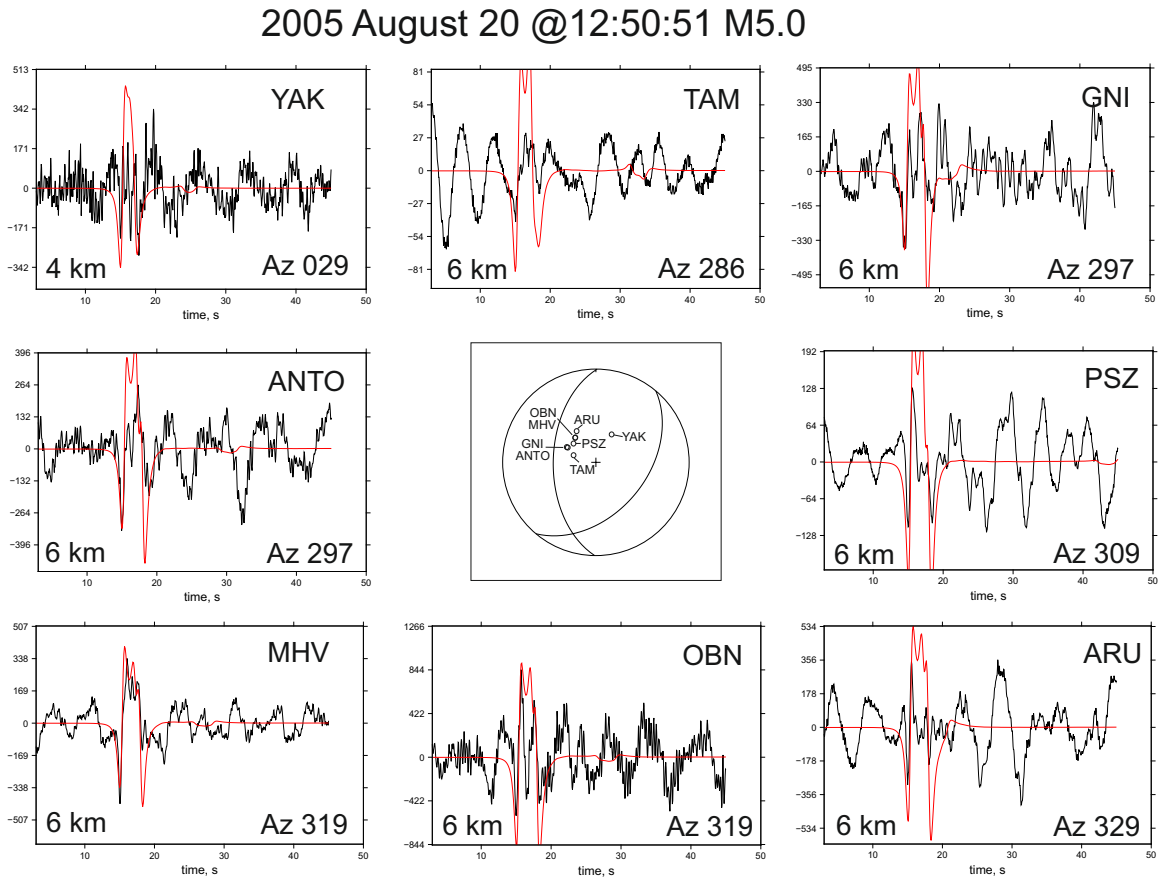

Figure S2. Unfiltered broadband waveforms (black) and synthetics (red) for the event on 2005/8/20. Synthetic waveforms are calculated using the mechanism shown, taken from our rCMT results, and with source depths as shown on the each panel. Synthetics are manually aligned with the *P*-wave onset.

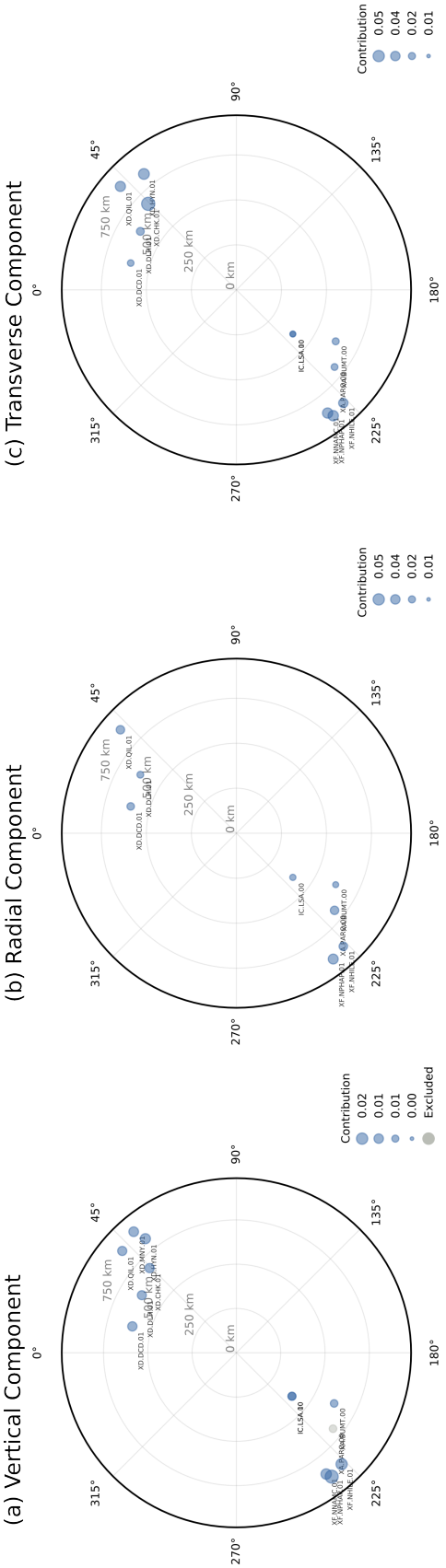

Figure S3. As in Figure S1, but for the earthquake on 2003/2/11.

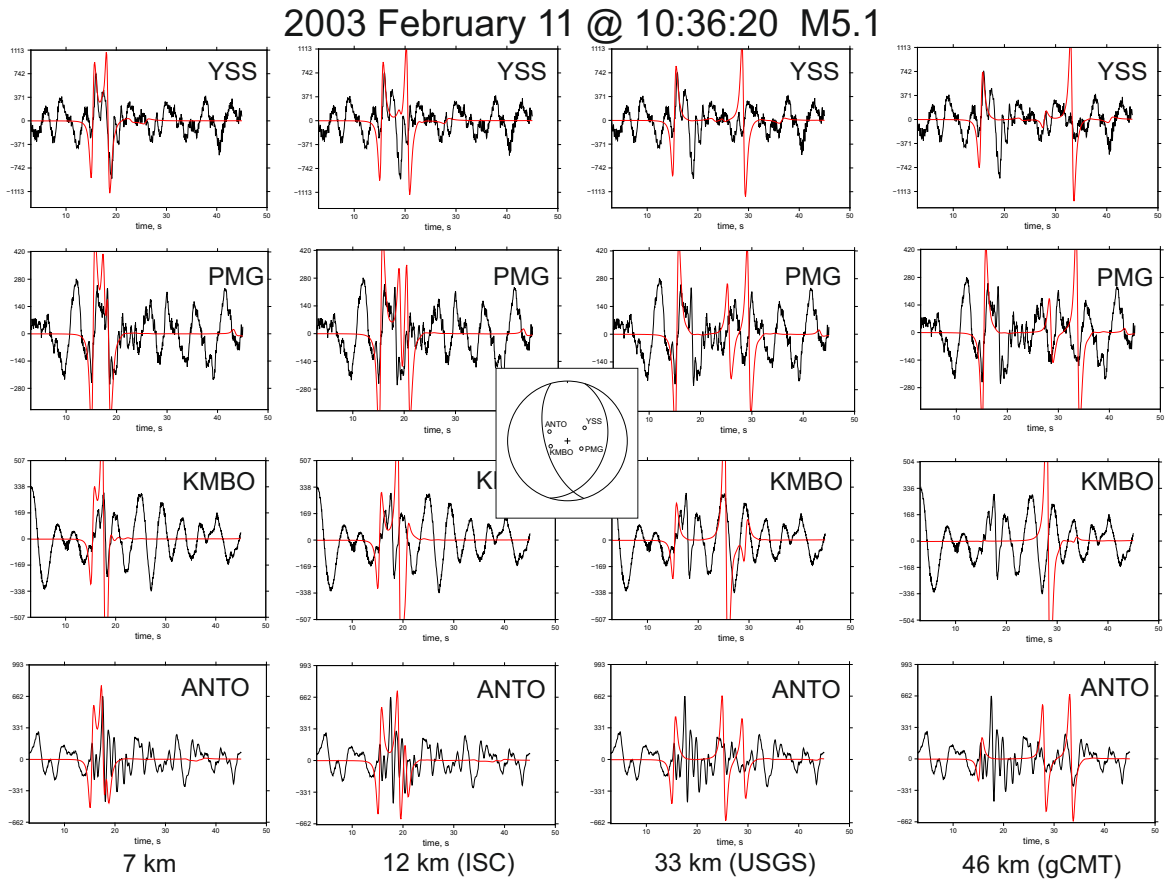

Figure S4. Unfiltered broadband waveforms (black) and synthetics (red) for the event on 2005/8/20. Synthetic waveforms are calculated using the mechanism shown, taken from our rCMT results. Each column shows waveforms from the same four stations, with synthetics calculated using the a source depth determined by our relocation (column 1), the ISC location (column 2), the NEIC location (column 3), the gCMT location (column 4) . Synthetics are manually aligned each time with the P-wave onset.

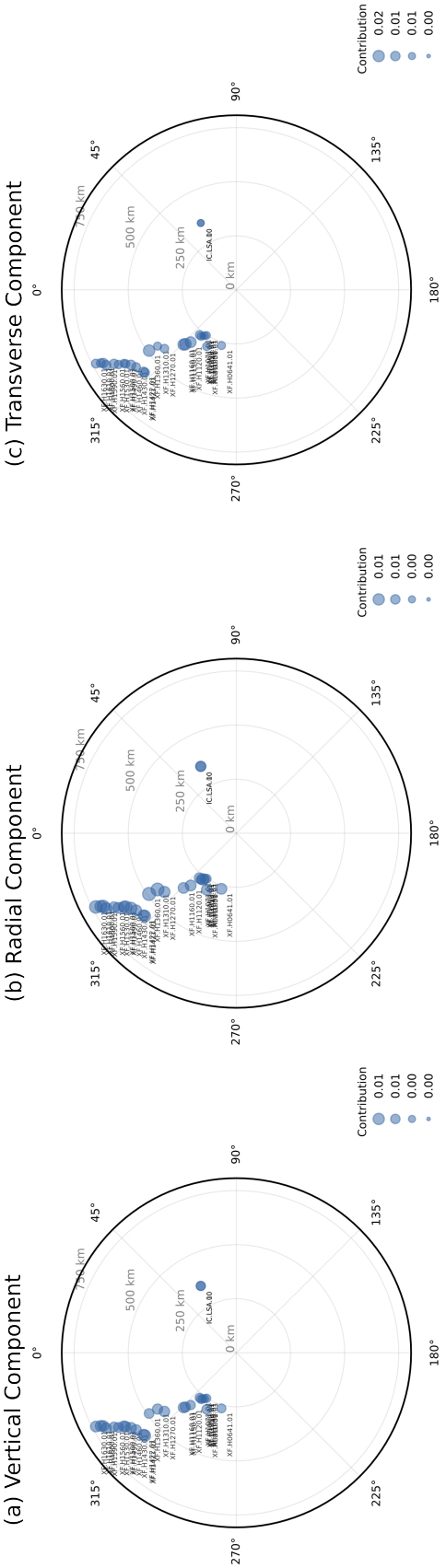

Figure S5. As in Figure S1, but for the earthquake on 2005/3/26

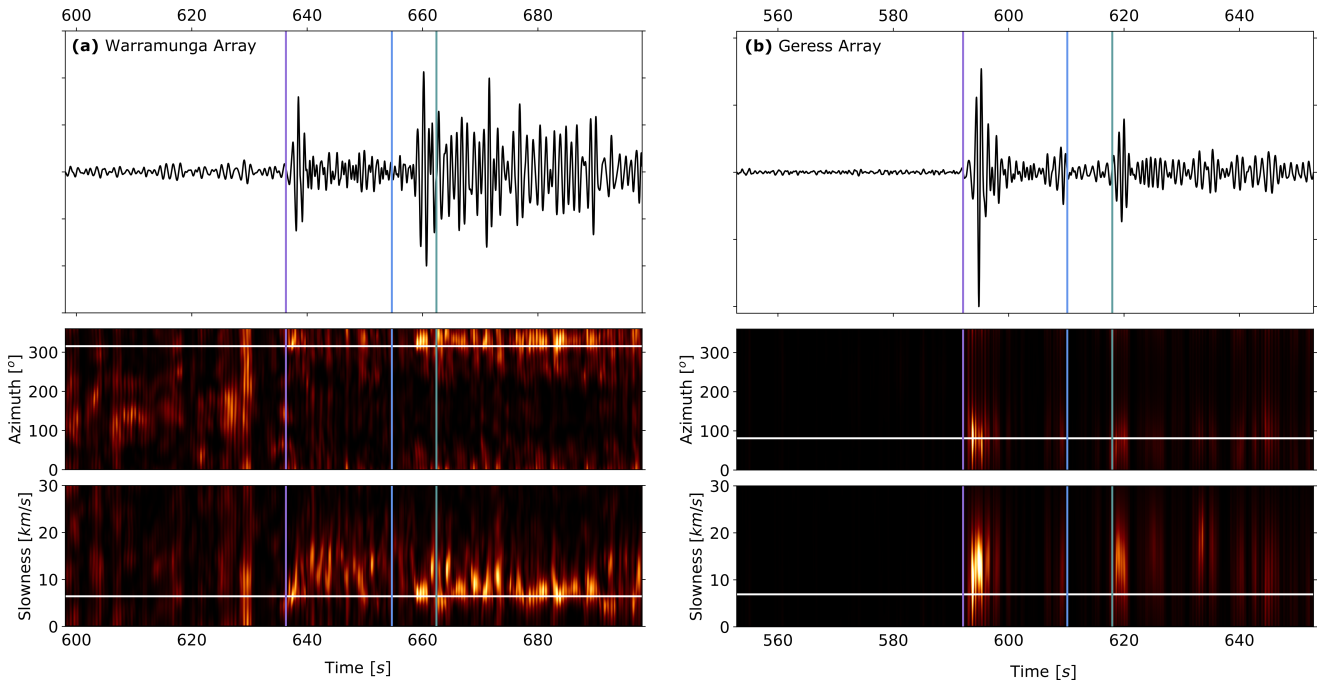

Figure S6. Array processing results for the 2005/3/26 event from arrays at (a) Warramunga, Australia; (b) GERESS, Germany. For each array, the upper panel shows the array beam using the predicted back azimuth and slowness. Lower panels show sweeps through back azimuth and slowness space, with the colour scale indicating beam power. White horizontal lines show the predicted back azimuth and slowness. On each panel, vertical lines show P (purple), pP (blue), and sP (green) arrivals, using the centroid depth from the gCMT catalogue (69.6 km). The arrival time for P is manually re-picked.

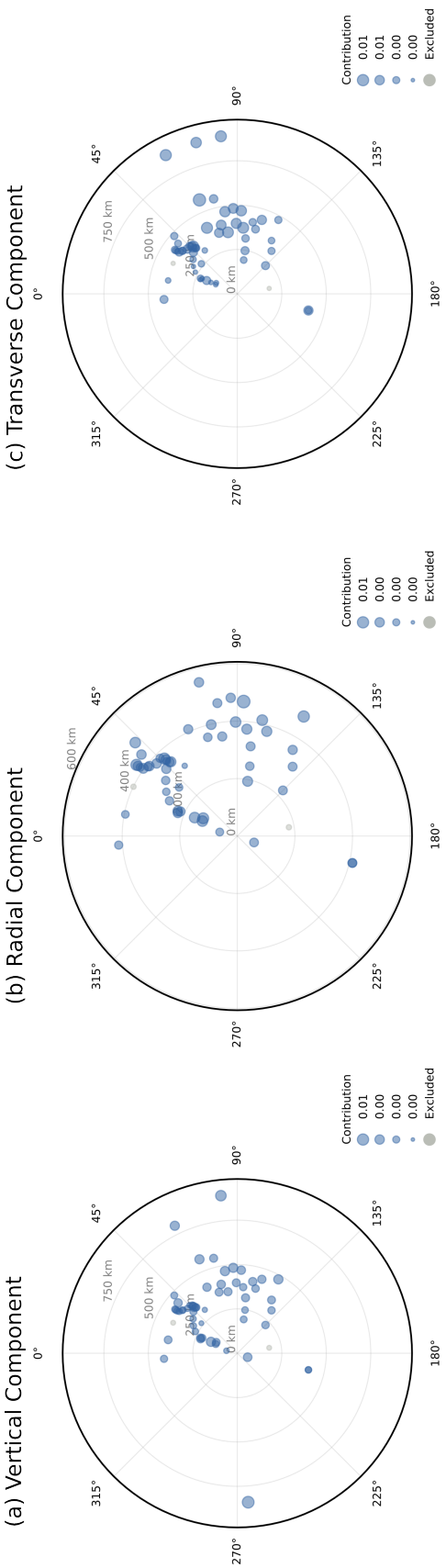

Figure S7. As in Figure S1, but for the earthquake on 2008/6/19.

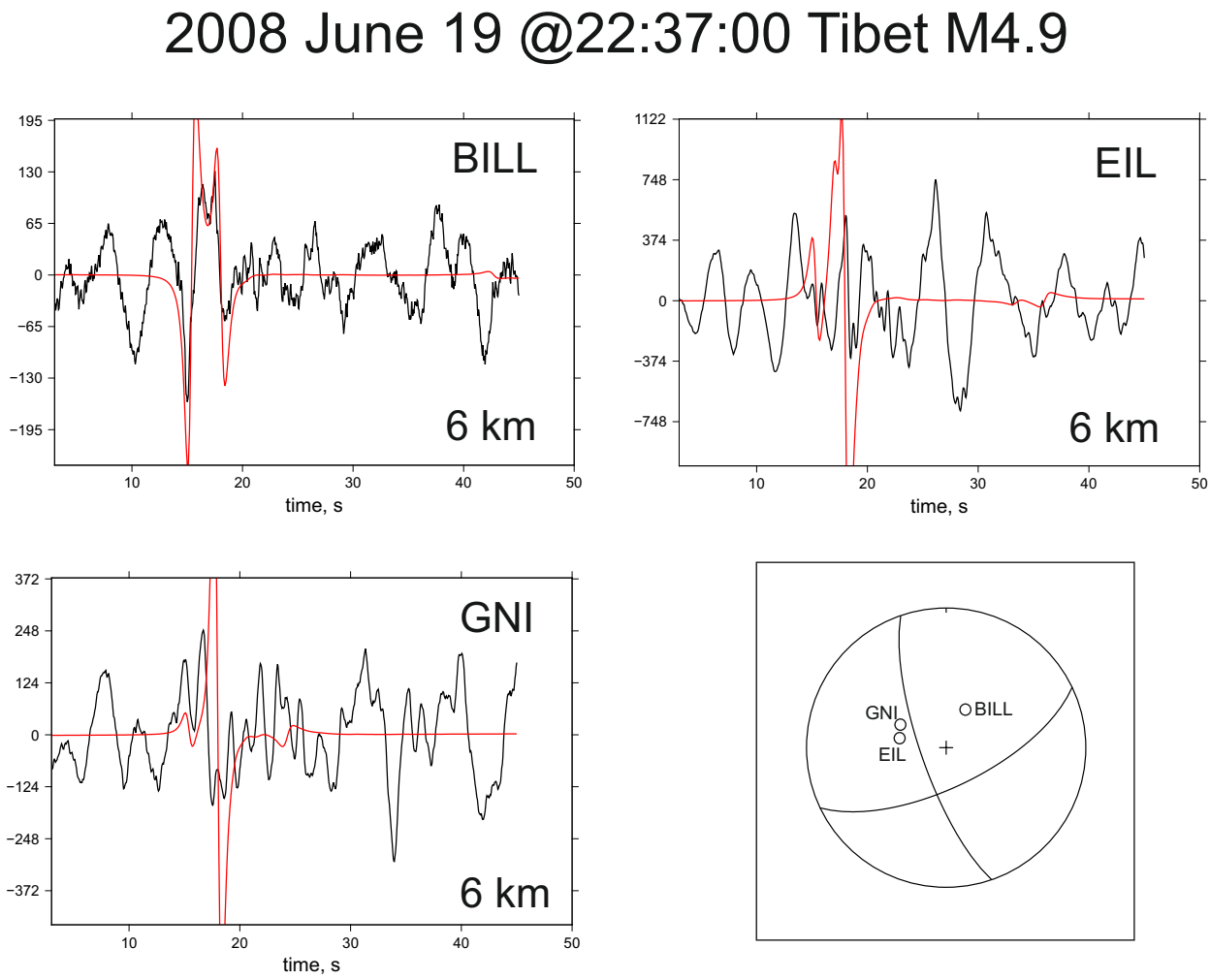

Figure S8. Unfiltered broadband waveforms (black) and synthetics (red) for the event on 2008/6/19. Synthetic waveforms are calculated using the mechanism shown, taken from our rCMT results, and with source depths as shown on the each panel. Synthetics are manually aligned with the P-wave onset.

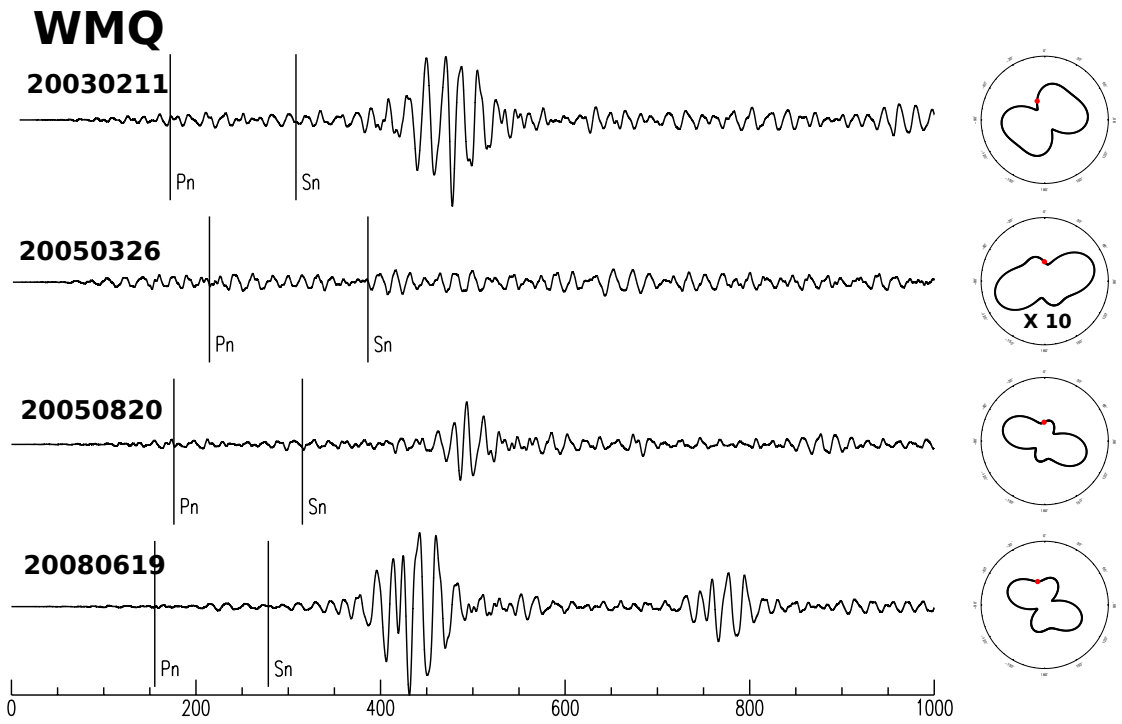

Figure S9. Rayleigh waves at the station IC.WMQ for all four events. Lefthand panels show waveforms, filtered around 0.05 Hz. Body wave arrivals are indicated by . Arrivals between 600 and 800 seconds are the Rayleigh waves. Righthand panels shown calculated Rayleigh wave radiation patterns based on our revised location and mechanism, with the red point indicating the azimuth and expected amplitude of IC.WMQ. Note that the radiation pattern for 2005/03/26 is magnified by a factor of 10, in order to be visible alongside the other radiation patterns.

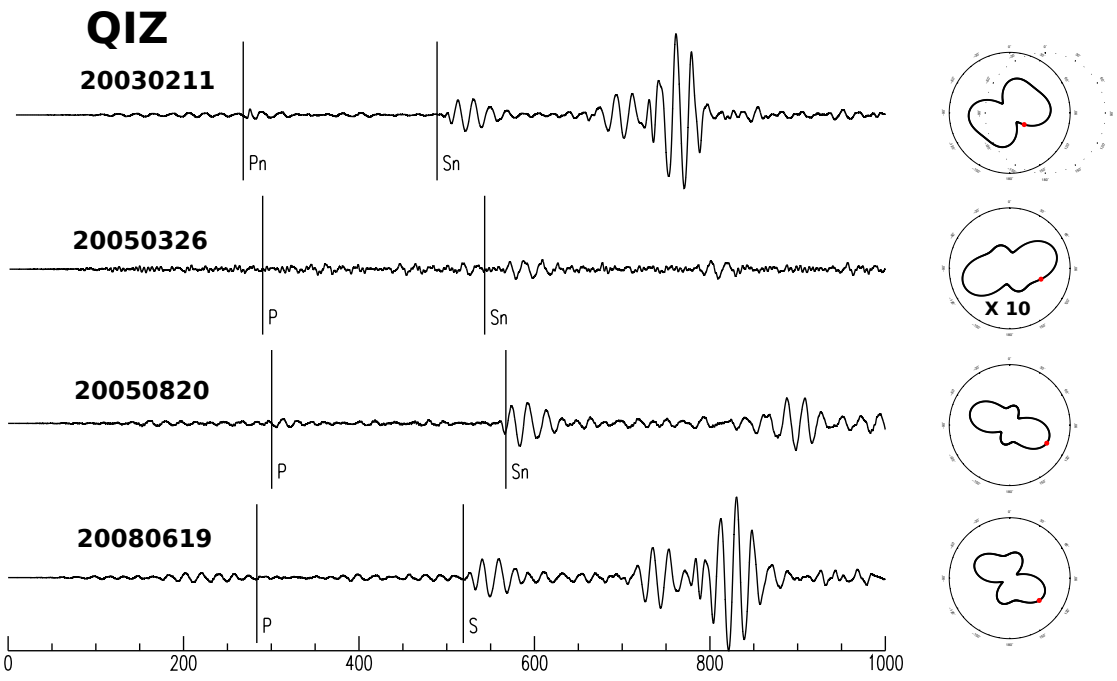

Figure S10. Rayleigh waves at the station IC.QIZ for all four events. Lefthand panels show waveforms, filtered around 0.05 Hz. Body wave arrivals are indicated by . Arrivals between 600 and 800 seconds are the Rayleigh waves. Righthand panels shown calculated Rayleigh wave radiation patterns based on our revised location and mechanism, with the red point indicating the azimuth and expected amplitude of IC.QIZ. Note that the radiation pattern for 2005/03/26 is magnified by a factor of 10, in order to be visible alongside the other radiation patterns.

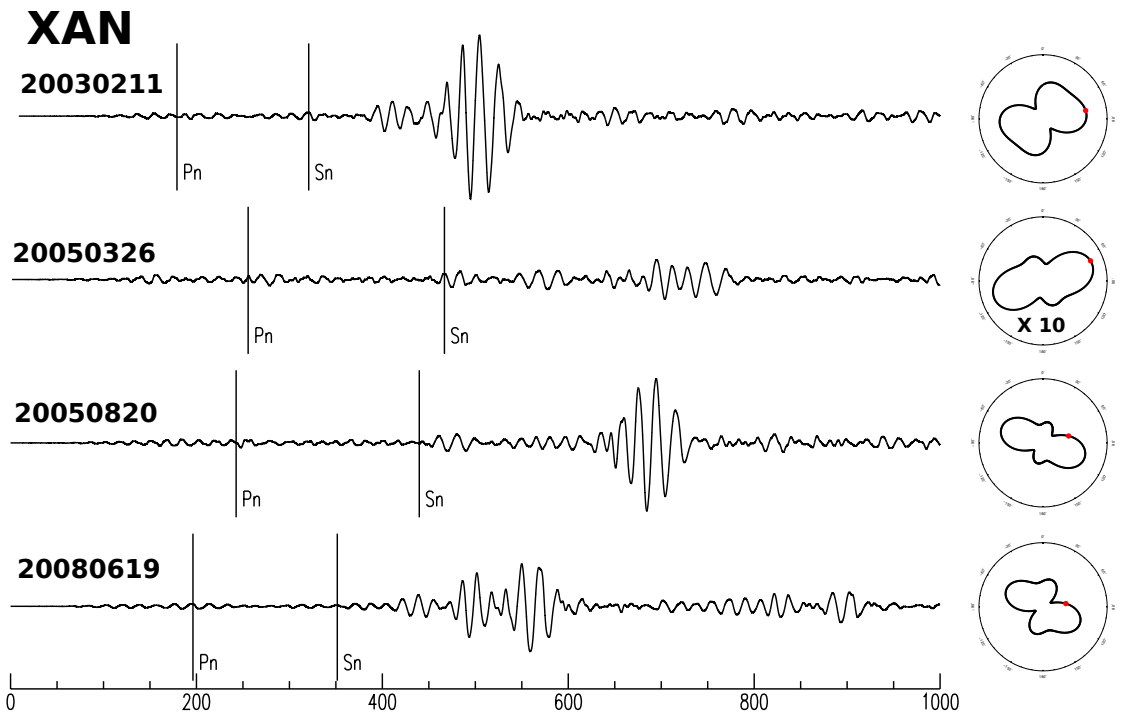

Figure S11. Rayleigh waves at the station IC.XAN for all four events. Lefthand panels show waveforms, filtered around 0.05 Hz. Body wave arrivals are indicated by . Arrivals between 600 and 800 seconds are the Rayleigh waves. Righthand panels shown calculated Rayleigh wave radiation patterns based on our revised location and mechanism, with the red point indicating the azimuth and expected amplitude of IC.XAN. Note that the radiation pattern for 2005/03/26 is magnified by a factor of 10, in order to be visible alongside the other radiation patterns.

Table S1. Centroid-moment-tensor solutions for the four reanalyzed earthquakes.

No.	Centroid Parameters													Half Drtn	Scale Factor 10^{ex}	M_0	Elements of Moment Tensor					
	Date			Time				Latitude		Longitude		Depth										
	Y	M	D	h	m	sec	δt_0	λ	$\delta\lambda_0$	ϕ	$\delta\phi_0$	h	δh_0				M_{rr}	$M_{\theta\theta}$	$M_{\phi\phi}$	$M_{r\theta}$	$M_{r\phi}$	$M_{\theta\phi}$
1	2003	2	11	10	36	22.3±0.2	2.7	32.52±.02	0.00	93.75±.01	-0.01	17.9± 0.6	6.2	0.8	23	5.1	-3.82±0.16	-0.37±0.10	4.19±0.11	-0.50±0.29	2.83±0.25	1.49±0.08
2	2005	3	26	20	32	16.3±0.4	5.3	28.07±.03	-0.18	88.02±.03	0.12	49.1± 3.3	-5.6	0.6	23	1.7	-0.48±0.19	-0.66±0.12	1.14±0.11	-0.30±0.08	-0.93±0.08	-0.96±0.07
3	2005	8	20	12	50	49.3±0.3	0.8	31.22±.03	0.04	88.25±.02	0.20	20.3± 1.1	-8.8	0.6	23	2.1	-1.86±0.16	-0.33±0.09	2.19±0.10	0.00±0.23	0.39±0.14	0.42±0.06
4	2008	6	19	22	36	59.3±0.2	1.7	33.20±.01	-0.01	92.21±.01	0.07	18.8± 0.9	4.8	0.7	23	3.0	-0.99±0.11	-1.38±0.08	2.38±0.08	-0.53±0.20	0.81±0.17	2.07±0.07

Table S2. Principal axes and best-double couple parameters.

No.	Scale Factor 10^{ex}	Principal Axes									M_0	Best Double Couple					
		T-axis			N-axis			P-axis				Plane 1			Plane 2		
		σ	δ	ξ	σ	δ	ξ	σ	δ	ξ		φ_s	θ	λ	φ_s	θ	λ
1	23	5.37	16	283	-0.46	15	189	-4.91	68	57	5.1	35	32	-60	181	63	-107
2	23	1.80	19	71	-0.27	48	184	-1.54	35	327	1.7	114	50	-166	16	80	-41
3	23	2.30	5	279	-0.40	2	189	-1.90	84	76	2.1	12	40	-86	187	50	-93
4	23	3.36	7	293	-0.66	63	189	-2.69	26	26	3.0	67	67	-14	162	77	-156